Journal of Solid State Chemistry **168,** 11–17 (2002)
doi:10.1006/jssc.2002.9667

The n=2 Member of the New Layered Structural Family $Ba_{5+n}Ca_2Mn_{3+n}O_{3n+14}$ Derived from the Hexagonal Perovskite: $Ba_7Ca_2Mn_5O_{20}$

N. Floros, C. Michel, M. Hervieu,[1] and B. Raveau

Laboratoire CRISMAT, UMR 6508, CNRS/ISMRA, 6 boulevard du Maréchal Juin, 14050 CAEN Cedex 4, France

Received January 30, 2002; in revised form May 6, 2002; accepted May 28, 2002

A new manganese oxide $Ba_7Ca_2Mn_5O_{20}$, with an original structure derived from the 21 L hexagonal perovskite, has been synthesized and studied by XRPD and HREM. This rhombohedral phase ($R\bar{3}m$), with $a = 5.8207(2)$ Å and $c = 51.359(1)$ Å, consists of [BaO_3] (h and c) layers and [BaO_2] (c') layers with a $(hhcc'cc)_3$ stacking sequence. This structure is closely related to that of $Ba_8Ca_{1.8}Mn_{6.2}O_{23-\delta}$, containing identical blocks "$Ba_5Ca_2Mn_3O_{14}$" built up of layers of corner-sharing CaO_6 octahedra, MnO_6 octahedra and MnO_4 tetrahedra. Both oxides can be described as the members $n = 2$ and 3 of the new structural family $Ba_{5+n}Ca_2Mn_{3+n}O_{3n+14}$, which differs from the hexagonal perovskite family by its bidimensional character, due to the disconnection of the MnO_4 tetrahedra layers. The charge distribution of manganese, Mn^{3+}/Mn^{4+} in octahedra and Mn^{5+} in tetrahedra is a particular feature of this structure.

INTRODUCTION

Barium manganese oxides, with the generic formula $BaMnO_3$ form a large family of polytypes, called hexagonal perovskites [see for a review Refs. (1–3)]. The structures of these oxides derive from the cubic perovskite: they consist of identical hexagonal [BaO_3] layers parallel to $(111)_p$ (suffix p refers to the unit cell of the cubic perovskite), forming similar octahedral sites. They differ from each other by the stacking of the [BaO_3] layers which exhibit a cubic "***c***" character when the layers of octahedra share their apices like in the cubic perovskite and a hexagonal "***h***"-type character when they share their faces. As a result, numerous polytypes can be synthesized, depending on the ratio of hexagonal/cubic layers, by varying the thermal conditions of synthesis, but also by replacing barium by strontium, or by substituting different elements for manganese (4–9).

[1] To whom correspondence should be addressed. Fax: 33-231-95-16-00. E-mail: hervieu@ismra.fr.

The introduction of a smaller alkaline earth cation such as calcium besides barium is of great interest since it is susceptible to induce an oxygen deficiency leading to the formation of MnO_5 pyramids (10–12), but also to derivatives where calcium is in octahedral coordination (13, 14). Recently, we synthesized a barium manganese oxide $Ba_8Ca_{1.8}Mn_{6.2}O_{23-\delta}$ (15–17) with an original structure (Fig. 1a) closely related to the ideal 16L polytype (Fig. 1b). Like the latter, it is built up from [BaO_3] ***h*** and ***c*** layers and thus forms quadruple layers of face-sharing MnO_6 octahedra. However, it differs from the 16L structure by the existence of oxygen deficient [BaO_2] layers with a cubic character (labeled ***c***′). As a consequence, each quadruple layer of corner-sharing MnO_6 octahedra of the 16L-$BaMnO_3$ structure is replaced by two double layers of corner-sharing CaO_6 octahedra and MnO_4 tetrahedra. In this new framework, the two successive tetrahedral layers are disconnected, giving to the structure a bidimensional character, in contrast to the hexagonal perovskites.

The close relationships between $Ba_8Ca_{1.8}Mn_{6.2}O_{23-\delta}$ and the different $BaMnO_3$ polytypes suggest the possibility to generate new structures by varying the thickness of the manganese octahedral layers. We have thus revisited the Ba–Ca–Mn–O system. In the present paper, we describe the original structure of a new phase $Ba_7Ca_2Mn_5O_{20}$, closely related to the hexagonal perovskite 21L—polytype. We show that this oxide, and the previously obtained $Ba_8Ca_{1.8}Mn_{6.2}O_{23}$ phase can be described as $n = 2$ and 3 members of a new family of layered structures with the generic formula $Ba_{5+n}Ca_2Mn_{3+n}O_{3n+14}$.

EXPERIMENTAL SECTION

Chemical Synthesis and Analysis

The title compound was prepared in an alumina crucible starting from $BaCO_3$, $CaCO_3$ and Mn_2O_3 intimately mixed and heated in air at 900°C for 2 days up to a complete

0022-4596/02 $35.00

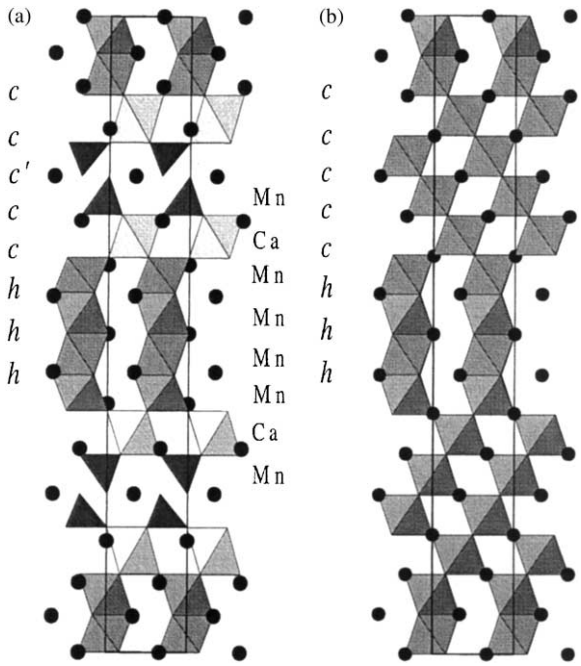

FIG. 1. Structure of (a) $Ba_{1.8}Ca_{1.8}Mn_{8.2}O_{23}$ showing the stacking sequence $(\boldsymbol{hhhccc'cc})_2$, (b) the 16L ideal polytype, showing the stacking sequence $(\boldsymbol{hhhccccc})_3$.

decarbonation of the samples. After regrinding, the powders were pressed into bars, placed at 800°C and heated up to 1400°C, with a soak time of 36 h at this temperature and an intermediate dwell of 12 h at 1200°C. The samples were then cooled down to 800°C in 2 h and then quenched to room temperature.

For each of the samples, numerous crystallites were analyzed by energy dispersive spectroscopy (EDS), using $BaMnO_{3-x}$ and $CaMnO_3$ as standards. Starting from the stoichiometric compositions, i.e., Ba:Ca:Mn = 7:2:5, a multiphasic sample was systematically observed due to the fact that $BaCO_3$ reacts with the alumina crucible to form barium aluminate, the latter being entered into the alumina crucible, as determined by EDS analysis. Thus, an excess $BaCO_3$ was introduced in order to saturate the crucible with barium. For a nominal composition Ba:Ca:Mn = 9:2:5, a perfectly single-phased sample was obtained. The EDS analysis was carried out for more than 140 crystallites; the Ba/Ca/Mn ratio is highly constant and leads to the cationic composition "$Ba_7Ca_2Mn_5$" (the standard deviation is of the order of a few percents). No other impurity, and, in particular, no trace of aluminum was detected, demonstrating that the excess of barium had entered into the crucible, but that there was no contamination of the sample by the crucible.

The oxygen ratio, determined by redox titration is 20.0(1) per formula unit leading to the composition $Ba_7Ca_2Mn_5O_{20}$, i.e., involving an average oxidation state close to +4.4 for manganese.

Structural and Magnetic Characterization

Samples for transmission electron microscopy were prepared by crushing the bars in *n*-butanol and the small crystallites in suspension were deposited onto a holey carbon film, supported by a nickel grid. The electron diffraction (ED) study was carried out at room temperature with a JEOL 200CX electron microscope. High-resolution electron microscopy (HREM) was performed with a TOPCON 002B microscope with a point resolution of 1.7 Å (acceleration voltage = 200 kV, spherical aberration = 0.4 mm). Energy dispersive spectroscopy (EDS) analyses were systematically carried out, both electron microscopes being equipped with KEVEX analyzers.

The X-ray powder diffraction (XRPD) data were collected at room temperature in the range $10° \le 2\theta \le 130°$ by increment of 0.02° in 2θ with a Philips X'PERT PRO diffractometer equipped with a rotating sample holder and working with the Cu$K\alpha$ radiation. Data were analyzed by the Rietveld method using the computer program Fullprof (18).

The magnetization measurements versus temperature were registered on warming from 10 to 400 K with a Quantum Design SQUID magnetometer in a magnetic field of 3000 G, which was applied at 10 K after zero-field cooling.

RESULTS AND DISCUSSION

Electron Diffraction and High-Resolution Electron Microscopy Study

The reconstruction of the reciprocal space was carried out by tilting around $\boldsymbol{c}^*$. It evidenced a rhombohedral lattice with $a \approx 5.8$ Å and $c \approx 51$ Å. The conditions limiting the reflection are $-h + k + l = 3n$, compatible with the space groups $R3$, $R32$, $R3m$, $R\bar{3}$ and $R\bar{3}m$. [001] and [010] ED patterns are given in Figs. 2a and 2b.

Considering that the average thickness of the barium–oxygen layers is around 2.4 Å in the $BaMO_{3-x}$ hexagonal perovskites, a structure closely related to that of the hexagonal perovskite 21L polytype (Fig. 3a) seems probable. A HREM investigation was then carried out in order to determine the layer stacking mode (19). The stacking sequence can be easily determined from the [110] images, especially for the focus values where the high electron density zones appear as bright dots, since they directly reveal the positions of the Ba and O columns. The images are built of straight and broken segments that correspond, respectively, to cubic (***c***) and hexagonal layers (***h***). Such an image recorded for $Ba_7Ca_2Mn_5O_{20}$ is given in Fig. 4 and it

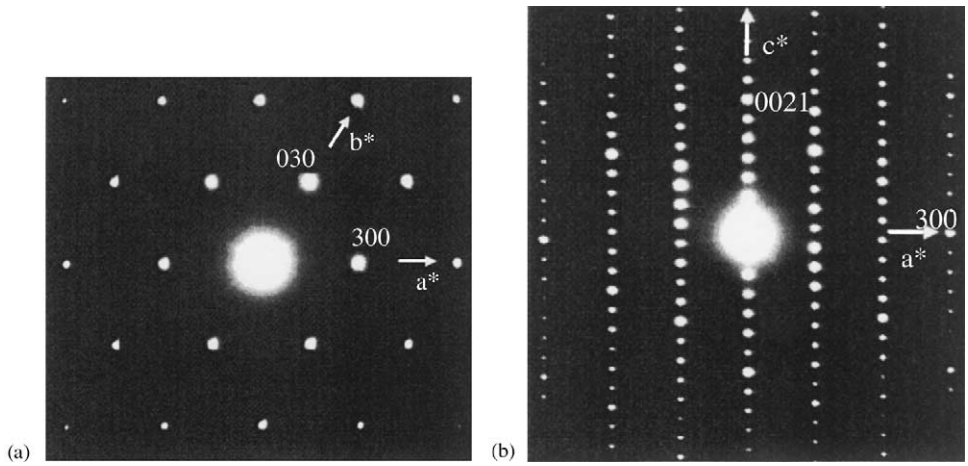

FIG. 2. $Ba_7Ca_2Mn_5O_{20}$: (a) [001] and (b) [010] ED patterns.

clearly appears that it exhibits a great similarity with those previously observed for $Ba_8Ca_{1.8}Mn_{6.2}O_{23}$ (15). The common part of the contrast consists of infinite parallel staircase lines built up of segments of seven aligned bright dots, which correspond to cubic stacking of five adjacent barium–oxygen layers in the two oxides. Moreover, the central dot of this cubic block exhibits an elongated contrast slightly weaker than that observed for the other dots. The latter feature was analyzed in $Ba_8Ca_{1.8}Mn_{6.2}O_{23}$ as the creation of oxygen vacancies in the central barium–oxygen layer (17), leading to tetrahedral manganese layers. Thus, these seven dot segments can be identified as the signature of identical cubic stacking built up of one central BaO_2 layer of ***c***′-type sandwiched between two double $[BaO_3]$ layers of ***c***-type, according to the sequence "***ccc′cc***." The straight segments of the cubic blocks alternate with broken segments of bright dots, associated to an hexagonal stacking of the layers. The two structures differ by the number of $[BaO_3]$ layers of hexagonal ***h*** type. In the title $Ba_7Ca_2Mn_5O_{20}$ compound, two ***h***-type $[BaO_3]$ layers are observed, against three ***h***-type $[BaO_3]$ layers in $Ba_8Ca_{1.8}Mn_{6.2}O_{23-\delta}$ (15, 17). The sequence between ***c***, ***c***′ and ***h*** layers is imaged in a mirror along [100] in $Ba_8Ca_{1.8}Mn_{6.2}O_{23}$, leading for this phase to the stacking $(\boldsymbol{hhhccc'cc})_2$ (Fig. 1a), whereas it is shifted by $\mathbf{a}/3$ along [100] in $Ba_7Ca_2Mn_5O_{20}$ (Fig. 4) leading to the stacking $(\boldsymbol{hhccc'cc})_3$ (Fig. 3b).

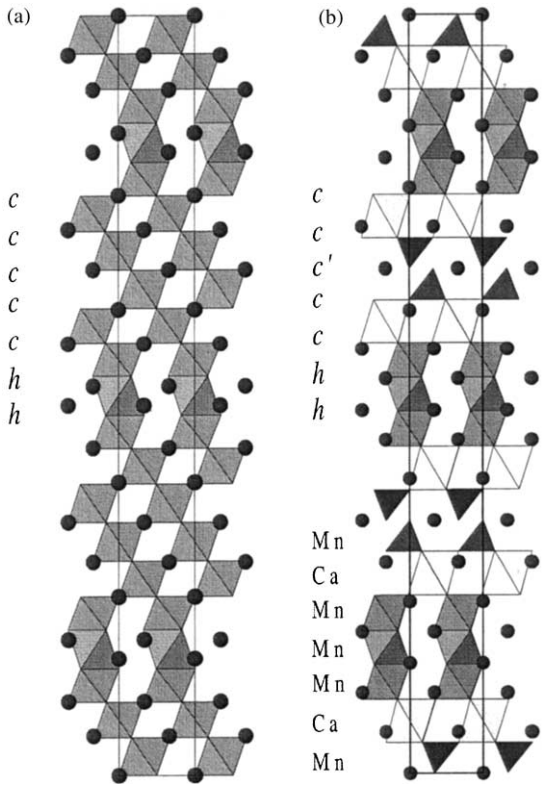

FIG. 3. Structure of (a) the ideal 21L hexagonal perovskite polytype showing the stacking sequence $(\boldsymbol{hhccccc})_3$ and (b) the oxide $Ba_7Ca_2Mn_5O_{20}$ showing the stacking sequence $(\boldsymbol{hhccc'cc})_3$.

The simulated images, calculated by varying the focus value and crystal thickness using the positional parameters refined from X-ray diffraction data (Table 1), fit with the experimental focus series. This is illustrated with the image calculated for a focus close to −60 nm and a crystal thickness close to 23 Å superimposed in Fig. 4. One should also note that, as in the $Ba_8Ca_{1.8}Mn_{6.2}O_{23}$ compound, no stacking fault has been observed on the several $Ba_7Ca_2Mn_5O_{20}$ crystals which have been studied.

X-Ray Diffraction Refinement

In order to confirm the structural model determined by HREM, a crystal structure was carried out from powder X-ray diffraction data. The most symmetric space group ($R\bar{3}m$)

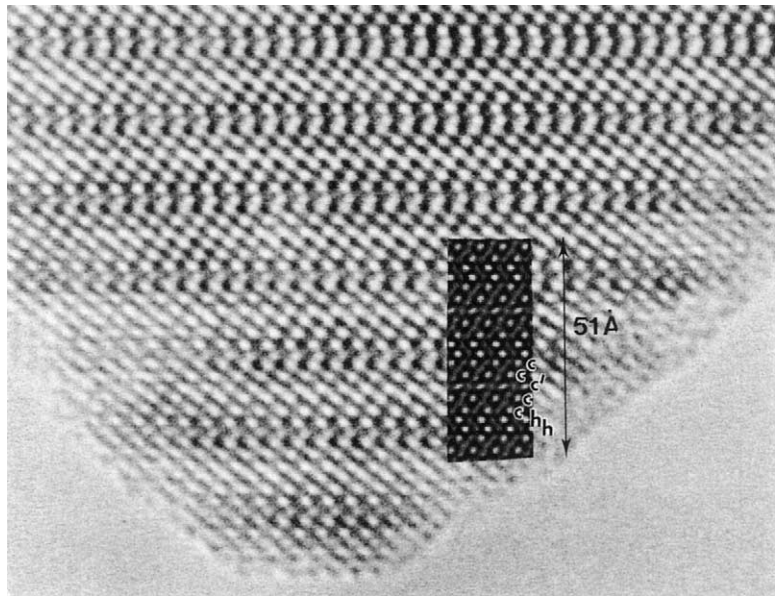

FIG. 4. HREM [110] images of $Ba_7Ca_2Mn_5O_{20}$. The simulated image has been calculated for the positional parameters listed in Table 1, focus value −60 nm and crystal thickness 23 Å.

was considered for the ideal stacking sequence ***(ccccchh)*$_3$**. Twelve atomic positions are necessary to describe this ideal model built of [BaO_3] layers and M cations (M = Mn or Ca) occupy four crystallographic sites. The atomic positions determined for $Ba_8Ca_{1.8}Mn_{6.2}O_{23}$ from single-crystal data (16) were used as a starting model for the structure determination. But, in a first step, we assumed that calcium and manganese atoms were randomly distributed over the four cationic sites and that the oxygen sites were fully occupied, as in the 21L hexagonal polytype. To reduce the number of structural parameters, the same atomic displacement factor was attributed to each kind of atoms (Ba, O or M). In these conditions, the refinements lead to a R-Bragg value of 8.65%.

However, for the above refinements, a too high atomic displacement B factor was obtained for the oxygen atoms ($B \approx 2$ Å^2). From these results, the B factor of each oxygen atom was refined separately. We observed that the B factors of all the oxygen atoms converged to a reasonable value except for O(4) (9e: $\frac{1}{2}, 0, 0$) which exhibits a high B factor ($B_{O(4)} \approx 14$ Å^2) strongly suggesting a wrong atomic position for this atom. Fourier difference maps were calculated at $z = 0$ and two residues were observed at $(x = \frac{1}{3}; y = \frac{2}{3})$ and $(x = \frac{2}{3}; y = \frac{1}{3})$ instead of $(x = \frac{1}{2}; y = 0)$, $(x = 0; y = \frac{1}{2})$ and $(x = \frac{1}{2}; y = \frac{1}{2})$ (Fig. 5). These new coordinates lead to a different atomic position for O(4): $6n(0, 0, z)$ with $z \approx \frac{1}{3}$. In the structure, this change corresponds to a replacement at $z \approx 0, \frac{1}{3}, \frac{2}{3}$ of a cubic c [BaO_3] layer by a cubic [BaO_2] layer noted c', in agreement with the HREM observations. Considering this new atomic position and the calcium/manganese distribution (see below), the refinement converges for a R-Bragg value of 6.2%. The structural parameters are given in Table 1 and the difference X-ray pattern attests of the goodness of fit (Fig. 6).

Although the X-ray scattering factors of calcium and manganese cations are very close, two points about the Mn/Ca distribution in the structure can be discussed considering the metal–oxygen distances given in Table 2.

TABLE 1
Structural Parameters for $Ba_7Ca_2Mn_5O_{20}$

Atom	Site	x	y	z	B (Å^2)
Ba(1)	6c	0	0	0	0.10(2)
Ba(2)	6c	0	0	0.1460(1)	0.10(2)
Ba(3)	6c	0	0	0.2268(1)	0.10(2)
Ba(4)	6c	0	0	0.3885(1)	0.10(2)
M_1[a]	6c	0	0	0.0746(4)	0.1(1)
M_2[b]	6c	0	0	0.4509(2)	0.1(1)
M_3[b]	3b	0	0	$\frac{1}{2}$	0.1(1)
M_4[b]	6c	0	0	0.6970(1)	0.1(1)
O(1)	18h	0.1784(5)	0.8215(5)	0.0970(3)	0.54(6)
O(2)	18h	0.1492(2)	0.8507(2)	0.4772(3)	0.54(6)
O(3)	18h	0.4935(5)	0.5064(5)	0.3752(2)	0.54(6)
O(4)	6c	0	0	0.3365(4)	0.54(6)
	A (Å)	5.8207(2)		Space group	$R\bar{3}m$
	C (Å)	51.359(1)			
	R-Bragg	0.062		R_p	0.164
	χ^2	3.0		R_{wp}	0.177

[a] Site occupied by calcium.
[b] Sites occupied by manganese.

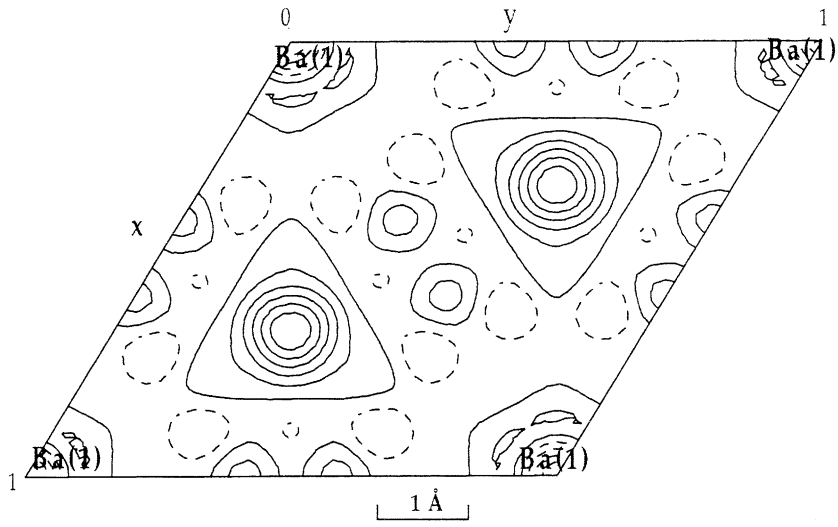

FIG. 5. Difference Fourier map at $z = 0$ for $Ba_7Ca_2Mn_5O_{20}$.

Firstly, the presence of the c' layers induces a tetrahedral coordination for M_4. It implies that this site is exclusively occupied by manganese. The M_4–O distances are close to those reported for Mn^{5+} in tetrahedral coordination. Secondly, while M_2–O and M_3–O distances correspond to those usually observed for Mn^{3+} or Mn^{4+}, the M_1–O distances (2.14 and 2.42 Å) are very unusual for manganese cations in octahedral coordination and strongly suggest that the M_1 site is occupied by calcium.

Thus, the structure of $Ba_7Ca_2Mn_5O_{20}$ (Fig. 3b) contains single layers of CaO_6 octahedra sharing their apices with single layers of MnO_4 tetrahedra practically identical to those observed for $Ba_8Ca_{1.8}Mn_{6.2}O_{23}$ (Fig. 1a). The two structures differ by the thickness of their octahedral layers of face-sharing MnO_6 octahedra, which are three and four octahedra thick, respectively.

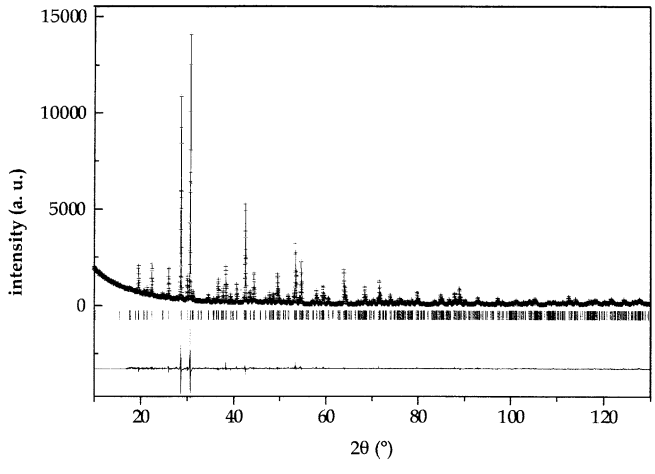

FIG. 6. Experimental (crosses), calculated and difference (solid lines) XRPD patterns of $Ba_7Ca_2Mn_5O_{20}$. Vertical bars show the Bragg angle positions.

Oxidation State of Manganese: Magnetic Measurements

The average oxidation state of manganese in this oxide of +4.4, deduced from the chemical formula is rather unusual and requires a magnetic study. The thermal variation of the molar susceptibility is plotted in Fig. 7. It does not show the presence of a magnetic order at low temperature. In the inset is the plot of χ_M^{-1} versus temperature. For $T > 250$ K, the variation is linear and can be fitted following a Curie–Weiss law with a θ_P value close to –200 K and a molar Curie constant of 7.3 e.m.u. mol^{-1} K. The negative value of θ_P indicates the

TABLE 2
Interatomic Distances in $Ba_7Ca_2Mn_5O_{20}$

Atom	–O	× n	d (Å)	Atom	–O	× n	d (Å)
M_1	–O(1)	× 3	2.14(1)	Ba(2)	–O(1)	× 3	3.09(1)
	–O(3)	× 3	2.42(1)		–O(2)	× 6	2.92(1)
					–O(2)	× 3	2.91(1)
M_2	–O(1)	× 3	1.89(1)				
	–O(2)	× 3	2.02(1)	Ba(3)	–O(1)	× 6	2.95(1)
					–O(2)	× 3	2.67(1)
M_3	–O(2)	× 6	1.91(1)		–O(3)	× 3	3.70(1)
M_4	–O(3)	× 3	1.72(1)	Ba(4)	–O(1)	× 3	2.66(1)
	–O(4)	× 1	1.72(2)		–O(3)	× 6	2.99(1)
					–O(4)	× 1	2.67(2)
Ba(1)	–O(3)	× 6	2.77(1)				
	–O(4)	× 6	3.36(1)				

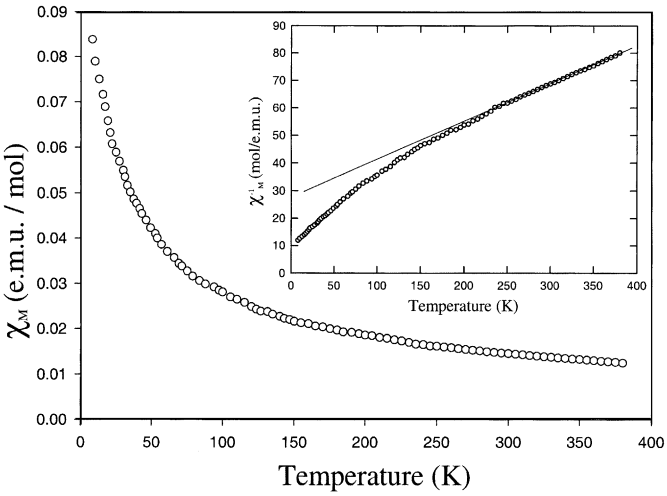

FIG. 7. Molar magnetic susceptibility versus temperature for $Ba_7Ca_2Mn_5O_{20}$. $\chi^{-1} = f(T)$ in the paramagnetic domain is given in the inset.

presence of antiferromagnetic interactions. At low temperature, the deviation from the Curie Weiss Law seems to be the signature of a weak ferromagnetic component, which could be due to quanted antiferromagnetism. In the linear domain, the calculated effective moment is 7.65 μ_B per formula unit. To explain this result, theoretical values were calculated for different oxidation states of manganese keeping the oxygen content of 20 per formula unit. The charge distribution that suits best with the experimental data, corresponds to the balance $3Mn^{4+}/2Mn^{5+}$, leading to a calculated μ_{eff} of 7.8 μ_B. Such a result is in perfect agreement with the structural study: it suggests that the octahedral sites (M_2 and M_3 sites) are fully occupied by Mn^{4+}, whereas the tetrahedral sites M_4 would be occupied by Mn^{5+} species.

CONCLUDING REMARKS

This study shows that starting from the ideal hexagonal 21L perovskite polytype, with formulation $BaMnO_3$, a new structural type $Ba_7Ca_2Mn_5O_{20}$ can be generated by calcium introduction. In fact, this structure is closely related to that of $Ba_8Ca_{1.8}Mn_{6.2}O_{23}$ (15–17) which derives from the ideal hexagonal 16L perovskite polytype.

The two structures of $Ba_8Ca_{1.8}Mn_{6.2}O_{23}$ (Fig. 1a) and of $Ba_7Ca_2Mn_5O_{20}$ (Fig. 3b), exhibit a common structural "cubic" block $Ba_5Ca_2Mn_3O_{14}$, which consists of the stacking of one $[BaO_2]$ ***c′***-type layer with four $[BaO_3]$ ***c***-type layers according to the sequence "***ccc′cc***." This stacking mode is also observed in the 21L structure, except that all the layers have the BaO_3 composition, so that the stacking sequence is "***c***". But, more importantly, these blocks differ from those observed in the 21L structure, by the fact that four layers of corner-sharing MnO_6 octahedra in these hexagonal perovskites, are replaced by two layers of CaO_6 octahedra and two layers of MnO_4 tetrahedra, according to the sequence "Mn_{oc}–Ca_{oc}–Mn_{te}–Mn_{te}–Ca_{oc}."

In the two structures the $Ba_5Ca_2Mn_3O_{14}$ blocks are stacked along c with blocks of composition $BaMnO_3$, which correspond to an hexagonal ***h***-type stacking of $[BaO_3]$ layers, as in the 16L- and 21L-type hexagonal perovskites. Thus, the two structures, $Ba_8Ca_{1.8}Mn_{6.2}O_{23}$ (Fig. 1c) and $Ba_7Ca_2Mn_5O_{20}$ (Fig. 3b), differ by the number n of layers of face-sharing MnO_6 octahedra, $n =$ 3 and 2, respectively. This description shows that $Ba_8Ca_{1.8}Mn_{6.2}O_{23}$ and $Ba_7Ca_2Mn_5O_{20}$ are the members, $n = 3$ and 2, of a new structural family with the generic formula $[Ba_5Ca_2Mn_3O_{14}][BaMnO_3]_n$ or $Ba_{5+n}Ca_2Mn_{3+n}O_{3n+14}$. In this series, the well-known 2L type $BaMnO_{3-x}$ (5) corresponds to the limit member $n = \infty$. Thus, other n members can be expected, whose symmetry and c parameters will depend on the stacking sequence. For odd n values, a $[\boldsymbol{ccc'cc(h)_n}]_2$ sequence is expected leading to an hexagonal symmetry with $c \approx 2 \times 2.4(n + 5)$ Å, whereas for even n values a $[\boldsymbol{ccc'cc(h)_n}]_3$ sequence is obtained leading to a rhombohedral symmetry with $c \approx 3(n+5)(2.4$ Å).

The bidimensionality of this structural type appears at the level of the $Ba_2Ca_5Mn_3O_{14}$ blocks, where the layers of MnO_4 tetrahedra are disconnected. This anisotropy is probably correlated with the two different valencies observed for manganese in these oxides, Mn(III)/Mn(IV) in the octahedra and Mn(V) in the tetrahedra. The route is now opened for the discovery of new materials with a layered structure, based on the hexagonal perovskite polytypes.

REFERENCES

1. A. F. Wells, *in* "Structural Inorganic Chemistry." Clarendon Press, Oxford.
2. C. N. R. Rao and B. Raveau, Colossal Magnetoresistance, Charge Ordering and Related Properties of Manganese Oxides. World Scientific Publishing, Singapore.
3. F. S. Galasso, *in* "Structure and Properties of Inorganic Solids," pp. 176–188. Pergamon Press, Oxford, 1970.
4. T. Negas and R. S. Roth, *J. Solid State Chem.* **3,** 323 (1970); ibid **1,** 409 (1970).
5. B. E. Gushee, L. Katz, and R. Ward, *Inorg. Chem.* **79,** 5601 (1957).
6. A. D. Potoff, B. L. Chamberland, and L. Katz, *J. Solid State Chem.* **8,** 234 (1973).
7. T. Takeda and S. T. Ohara, *J. Phys. Soc. Jpn* **37,** 275 (1974).
8. P. C. Donohue, L. Katz, and R. Ward, *Inorg. Chem.* **5,** 339 (1966).
9. Ph. Boullay, M. Hervieu, Ph. Labbé, and B. Raveau, *Mater. Res. Bull.* **32,** 35 (1997).
10. A. J. Jacobson and A. J. W. Horrox, *Acta Crystallogr. B* **32,** 1003 (1976).
11. J. M. Gonzalez-Calbet, M. Parras, J. M. Alonso, and M. Vallet-Regi, *J. Solid State Chem.* **106,** 99 (1993).
12. V. Caignaert, M. Hervieu, B. Domengès, N. Nguyen, J. Pannetier, and B. Raveau, *J. Solid State Chem.* **73,** 107 (1998).

13. J. Darriet, M. Drillon, G. Villeneuve, and P. Hagenmuller, *J. Solid State Chem.* **19,** 213 (1976).
14. H. W. Zandbergen and D. J. W. Ijdo, *Acta Crystallogr. C* **39,** 829 (1983).
15. N. Floros, C. Michel, M. Hervieu, B. Raveau. *Chem. Mater.* **10,** 3197 (2000).
16. N. Floros, M. Hervieu, C. Michel, O. Perez, and B. Raveau, *Solid State Sci.* **4,** 627 (2002).
17. W. Schuddink, G. Van Tendeloo, M. Hervieu, and B. Raveau, *Mat. Res. Bull.* **36,** 2689 (2001).
18. J. Rodriguez Carvajal, *in* Collected Abstracts of Satellite Meeting on Powder Diffraction of XVth. Congrress on International Union Crystallograph, Toulouse, 1990, p. 127.
19. J. L. Hutchison and A. J. Jacobson, *Acta Crystallogr. B* **31,** 1442 (1975); *J. Solid State Chem.* **20,** 417 (1977).